AIAA JOURNAL
Vol. 31, No. 5, May 1993

Calculation of Compressible Boundary Layers by a Hybrid Finite Element Method

Andrew J. Meade Jr.*
Rice University, Houston, Texas 77251

Preliminary results are presented of a finite element/finite difference method (semidiscrete Galerkin or SDG method) used to calculate compressible turbulent boundary-layer flow about airfoils, in which the group finite element scheme is applied to the Dorodnitsyn formulation of the boundary-layer equations. The finite element discretization across the layer yields a system of first-order ordinary differential equations in the streamwise direction. Linear elements are chosen for computational efficiency, while also providing adequate accuracy. The streamwise derivatives are solved by an implicit and noniterative finite difference marching scheme. Results are presented for low-speed laminar flow past a circular cylinder and past an NACA 0012 airfoil at zero angle of attack at a Mach number of 0.5. Also shown are results for compressible flow past a flat plate for a Mach number range of 0–10 and results for incompressible turbulent flow past a flat plate. All numerical solutions assume an attached boundary layer. The semidiscrete Galerkin method promises to be fast, accurate, and computationally efficient. The resulting computer code can also be applied to any smoothly connected airfoil shape without modification and can be coupled to any existing inviscid flow solver (portability).

Introduction

At present there are essentially two approaches to the numerical simulation of viscous flow past airfoils and wings: the fully viscous methods and the inviscid/viscous interaction methods. The fully viscous models require the solution of an approximation of the Navier-Stokes equations for the entire flowfield and therefore should simulate most of the physical mechanisms. However, in all cases the fully viscous models require large amounts of computer time and storage relative to the interaction methods. Unless extensive flow separation is present, the use of fully viscous models can be considered impractical for the design of most airfoils and wings, since hundreds of iterations are usually required at various flow conditions. Because of their relative speed and simplicity, the inviscid/viscous models are still in wide use in design and theoretical investigations.

The inviscid/viscous methods assume that the flowfield can be modeled as an outer inviscid region and a thin inner viscous region near the body surface. Solution of the inviscid region usually employs an Euler equation solver interacting with a model of the thin shear layer near the airfoil surface. Traditionally, the boundary-layer equations have been adopted for the viscous layer and solved using the finite difference methods.[1,2] However, the advantages of a finite element approach to the boundary-layer solution are gaining recognition. Both full finite element[3] methods and finite element/finite difference hybrid methods[4–7] have been applied to laminar and turbulent cases with considerable success.

A numerical method that takes advantage of the parabolic nature of the compressible boundary-layer equations[8] in a manner similar to that used by Refs. 6 and 7 for incompressible flow is presented here. The method applies a finite element/finite difference procedure (semidiscrete Galerkin method or SDG method), using group finite elements,[9] to a Dorodnitsyn formulation of the compressible boundary-layer approximations.[10] In contrast to Refs. 3–5 the Dorodnitsyn formulation allows the numerical method to automatically follow the boundary-layer growth and provides high spatial resolution near the body surface.

Dorodnitsyn Boundary-Layer Formulation—Equations of Motion

The viscous flow region, before separation from the body, is assumed to extend over a small distance normal to the surface. The equations of motion for steady, viscous, turbulent, compressible, and nonisentropic flow about a two-dimensional body are nondimensionalized in the following manner:

$$u = \frac{\tilde{u}}{a^*}, \quad v = \frac{\tilde{v}}{a^*}, \quad w = \frac{\tilde{w}}{a^*}, \quad U_\infty = \frac{\tilde{U}_\infty}{a^*}$$

$$p = \frac{\tilde{p}}{\rho_\infty a^{*2}}, \quad p_\infty = \frac{\tilde{p}_\infty}{\rho_\infty a^{*2}}, \quad \rho = \frac{\tilde{\rho}}{\rho_\infty}$$

$$a = \frac{\tilde{a}}{a^*}, \quad x = \frac{\tilde{x}}{L}, \quad y = \frac{\tilde{y}}{L}, \quad \mu = \frac{\tilde{\mu}}{\rho_\infty a^* L}$$

$$H = \frac{c_p T + \frac{1}{2}(\tilde{u}^2 + \tilde{v}^2)}{a^{*2}} \tag{1}$$

where $\tilde{a}$ is the local speed of sound, a^* the critical speed of sound, and H the dimensionless total (stagnation) enthalpy. The subscript ∞ indicates freestream conditions. The overbar and tilde denote dimensional variables that have been time averaged and mass weighted averaged,[11] respectively. The independent and dependent variables are written in terms of the orthogonal coordinate system shown in Fig. 1.

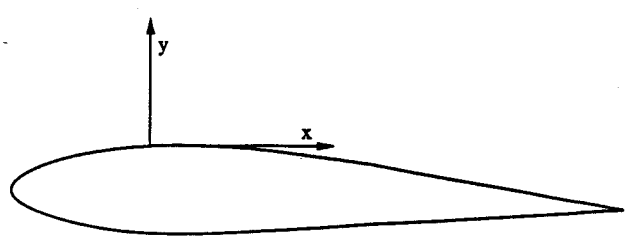

Fig. 1 Local coordinate system.

Presented as Paper 92-0524 at the AIAA 30th Aerospace Sciences Meeting and Exhibit, Reno, NV, Jan. 6–9, 1992; received Jan. 23, 1992; revision received Sept. 9, 1992; accepted for publication Sept. 20, 1992.

*Assistant Professor, Department of Mechanical Engineering and Materials Science. Member AIAA.

The gross effects of turbulence in the boundary layer are accounted for using the eddy-viscosity model[11]

$$\overline{\mu_t} = \frac{\bar{\rho}\overline{u'v'}}{\partial\bar{u}/\partial\bar{y}} \tag{2}$$

where the primes indicate the fluctuations of the variables from the time-averaged values.

For the inner region ($0 \leq y^+ \leq 350$), the van Driest[12] empirical formula is applied. In dimensionless form, the formula is written as

$$\frac{\bar{\mu}_t}{\bar{\mu}} = \kappa^2 (y^+)^2 \frac{\tau}{\tau_1} (1 - e^{-y^+/A^+})^2 \tag{3}$$

where

$$y^+ = \sqrt{\tau_1 \left(\frac{\rho}{C}\right)\left(\frac{p_\infty}{p_e}\right)\sqrt{\frac{u_\infty}{\mu_\infty}}} \left(\rho \int_0^1 \frac{1}{\rho\tau}\, du_2\right)$$

The variable τ_1 is the value of τ at the surface. The nondimensional dependent variable τ is derived from the Crocco transformation described by Eq. (14).

For the outer region ($350 \leq y^+$), the Clauser[13,14] empirical formula is used. The dimensionless formulation appears as

$$\frac{\bar{\mu}_t}{\bar{\mu}} = \kappa \left(\frac{\rho}{\rho_e}\right)\left(\frac{\rho}{C}\right)\left(\frac{p_\infty}{p_e}\right)\sqrt{\frac{u_\infty}{\mu_\infty}} \int_0^1 \left(\frac{\rho_e}{\rho} - u_2\right) \frac{1}{\tau}\, du_2 \tag{4}$$

where $\kappa = 0.016$ and $A^+ = A_0^+ = 26$ for a zero pressure gradient.

The dimensionless variable F is used as the turbulence parameter and is defined as

$$F = 1 - \frac{\overline{\mu_t}}{\bar{\mu}} \tag{5}$$

The Prandtl boundary-layer assumptions are then applied to give the resulting equations of motion:

Conservation of mass:

$$\frac{\partial}{\partial x}(\rho u) + \frac{\partial}{\partial y}(\rho v) = 0 \tag{6}$$

Conservation of x momentum:

$$\rho u \frac{\partial u}{\partial x} + \rho v \frac{\partial u}{\partial y} = -\frac{dp_e}{dx} + \frac{\partial}{\partial y}\left(\mu F \frac{\partial u}{\partial y}\right) \tag{7}$$

Conservation of energy:

$$\rho u \frac{\partial H}{\partial x} + \rho v \frac{\partial H}{\partial y} = \frac{1}{Pr}\frac{\partial}{\partial y}\left(\mu F \frac{\partial H}{\partial y}\right) + \left(1 - \frac{1}{Pr}\right)\frac{\partial}{\partial y}\left[\mu F \frac{\partial}{\partial y}\left(\frac{u^2}{2}\right)\right] \tag{8}$$

The Prandtl number Pr is assumed constant as are the specific heats c_v and c_p. The subscript e denotes conditions at the outer edge of the boundary layer.

Equations (6–8) can be simplified further. The independent variables x and y are replaced by ξ and η; and the dependent variables u, H, and v are replaced by u_2, s, and w_2, respectively. The new variables are defined as follows:

$$\xi = \frac{1}{U_\infty}\int_0^x u_e \frac{p_e}{p_\infty}\, dx, \quad \eta = \frac{u_e}{(U_\infty \mu_\infty)^{1/2}}\int_0^y \rho\, dy$$

$$\frac{\bar{\mu}}{\bar{\mu}_\infty} = \frac{\mu}{\mu_\infty} = C\frac{T}{T_\infty}$$

$$u_2 = \frac{u}{u_e}, \quad w_2 = \frac{U_\infty p_\infty}{u_e p_e} u_2 \frac{\partial\eta}{\partial x} + \left(\frac{U_\infty}{\mu_\infty}\right)^{1/2} \frac{\nu}{u_e}\frac{T_\infty}{T}$$

$$s = \left[1 - \frac{2H(\gamma - 1)}{(\gamma + 1)}\right]\left(\frac{1}{u_e^2}\right) \tag{9}$$

It is assumed that the variation of laminar viscosity across the boundary layer can be represented by a linear relation. A full explanation of the assumption is given by Chapman and Rubesin.[15]

The results of our various transformations and substitutions are the following:

Conservation of mass:

$$\frac{\partial u_2}{\partial\xi} + \frac{\partial w_2}{\partial\eta} = 0 \tag{10}$$

Conservation of x momentum:

$$u_2 \frac{\partial u_2}{\partial\xi} + w_2 \frac{\partial u_2}{\partial\eta} = l_1(1 - u_2^2) + C\frac{\partial}{\partial\eta}\left(F\frac{\partial u_2}{\partial\eta}\right) \tag{11}$$

Conservation of energy:

$$u_2 \frac{\partial s}{\partial\xi} + w_2 \frac{\partial s}{\partial\eta} + 2l_1 u_2 s = \frac{C}{Pr}\frac{\partial}{\partial\eta}\left(F\frac{\partial s}{\partial\eta}\right) + l_2\frac{\partial}{\partial\eta}\left(u_2 F \frac{\partial u_2}{\partial\eta}\right) \tag{12}$$

The simplification of the equations of motion is now complete. The three partial differential equations describing a two-dimensional, turbulent, and compressible boundary layer have been converted into a system of equations resembling the incompressible form.

The coefficients l_1 and l_2 are functions of the freestream conditions and/or the streamwise position ξ. The coefficients are defined as follows:

$$l_1 = \frac{1}{u_e}\frac{\partial u_e}{\partial\xi}, \quad l_2 = \frac{2C(\gamma - 1)}{(\gamma + 1)}\left(\frac{1}{Pr} - 1\right) \tag{13}$$

The differential equations (10–12) are transformed into an integral form using the method of weighted residuals.

The Crocco transformation [Eq. (14)] is applied to the integral equations to change the independent variable η to u_2,

$$u_2 = \int_0^\eta \tau\, d\eta \tag{14}$$

where

$$\tau = \frac{\partial u_2}{\partial\eta}$$

Explicit dependence on the variable w_2 can be eliminated by seeking weighted combinations of Eqs. (10–12). It is assumed that the general weighting function f vanishes at the outer edge of the boundary layer ($\eta = \infty$ or $u_2 = 1$) and is a function of the variable u_2 only. By multiplying Eq. (10) by f and adding to $df/du_2 \times$ Eq. (11) and integrating the transformed equation from zero to one, with respect to u_2, we obtain

$$\frac{d}{dx}\int_0^1 \frac{u_2 f}{\tau}\, du_2 = C\int_0^1 \frac{df}{du_2}\frac{\partial(F\tau)}{\partial u_2}\, du_2 + l_1\int_0^1 \frac{df}{du_2}\frac{(1 - u_2^2)}{\tau}\, du_2 - (w_2 f)\Big|_0^1$$

To permit a more physically oriented solution procedure, it is desirable to use the independent variable x in place of ξ. This

requires a change only in the coefficients. The preceding integral equation is rewritten as

$$\frac{d}{dx}\int_0^1 \frac{u_2 f}{\tau}\,du_2 = Cl_4 \int_0^1 \frac{df}{du_2}\frac{\partial(F\tau)}{\partial u_2}\,du_2$$

$$+ l_3 \int_0^1 \frac{df}{du_2}\frac{(1-u_2^2)}{\tau}\,du_2 - l_4(w_2 f)\Big|_0^1 \qquad (15)$$

where

$$l_3 = \frac{1}{u_e}\frac{du_e}{dx} \quad \text{and} \quad l_4 = \frac{u_e p_e}{U_\infty p_\infty}$$

The integral of the sum of $s \times f \times$ Eq. (10), $s \times df/du_2 \times$ Eq. (11), and $f \times$ Eq. (12), after replacing ξ with x, is equal to

$$\frac{d}{dx}\int_0^1 u_2 f\frac{s}{\tau}\,du_2 = \frac{Cl_4}{Pr}\int_0^1 f\frac{\partial}{\partial u_2}\left(F\tau\frac{\partial s}{\partial u_2}\right)du_2$$

$$+ l_3\int_0^1 (1-u_2^2)\frac{df}{du_2}\frac{s}{\tau}\,du_2 + l_4 l_2\int_0^1 f\frac{\partial}{\partial u_2}(u_2 F\tau)\,du_2$$

$$+ Cl_4\int_0^1 \frac{df}{du_2}s\frac{\partial(F\tau)}{\partial u_2}\,du_2$$

$$- 2l_3\int_0^1 u_2 f\frac{s}{\tau}\,du_2 - l_4(sw_2 f)\Big|_0^1 \qquad (16)$$

It is assumed that there is neither surface injection nor suction. Therefore v and, hence, w_2 are zero at the wall. Since w_2 and f are zero at the wall and the boundary-layer edge, respectively, w_2 no longer appears explicitly in the equations.

The three partial differential equations describing two-dimensional, turbulent, and compressible boundary layers [Eqs. (6–8)] have been converted into a system of two uncoupled integral equations. The Dorodnitsyn formulation of the equations of motion offers some significant advantages over the preceding simplified Eqs. (10–12).

First, the governing equations are in a weighted residual form. An array of error distribution techniques can be applied to force the integrals of the residuals weighted by a certain function to zero. In addition, the integral or "weak" formulation reduces the order of the continuity required for a function approximating the solution.[16] Second, by using u_2 as an independent variable across the boundary layer, the infinite domain of η has been replaced by a finite domain. The high gradients of the variables in y have been decreased, significantly resulting in high resolution of the dependent variables near the wall. This is of particular importance in turbulent flow. The use of u_2 as an independent variable also allows a uniform grid to be employed that automatically follows the growth of the boundary layer. The variable w_2 does not appear explicitly in the equations and can be recovered later. The shear stress τ is solved for directly and should be particularly accurate.

Finite Element/Finite Difference Method

Application of Finite Elements

To apply the finite element method, the general weighting function f must be replaced by a set of linearly independent functions f_k (for $k = 1, \ldots, N$). For this problem, the set f_k is written as

$$f_k = (1-u_2)\,\Phi_k \qquad (17)$$

where Φ_k is the interpolation function centered at a particular node k and is dependent only on u_2. The term $(1-u_2)$ is introduced to satisfy the requirement that f_k equals zero at the outer edge of the boundary layer.

The group finite element method differs from conventional finite elements in that combinations of dependent variables, in addition to the individual variables, are represented by piecewise continuous polynomials. The trial solutions for combinations of the dependent variables τ, F, and s are as follows:

$$\frac{1}{\tau} = \frac{1}{(1-u_2)}\sum_j^N \Phi_j b1_j, \qquad F\tau = (1-u_2)\sum_j^N \Phi_j b2_j$$

$$s = (1-u_2)\sum_j^N \Phi_j b3_j, \qquad \frac{s}{\tau} = \sum_j^N \Phi_j b4_j \qquad (18)$$

Substituting the trial solutions for τ, F, s, and f_k, Eqs. (15) and (16) are rewritten as

$$\sum_j^N G1_{kj}\frac{db1_j}{dx} = D1_k \qquad (19)$$

$$\sum_j^N G2_{kj}\frac{db4_j}{dx} = D2_k \qquad (20)$$

for $k = 1, \ldots, N$. The variables $D1_k$ and $D2_k$ represent the right-hand sides of Eq. (15) and (16), respectively. Linear elements were chosen for computational efficiency while also providing adequate accuracy. The finite element discretization yields two uncoupled sets of first-order ordinary differential equations in the streamwise direction. Note that with the substitution of the trial solutions using linear elements, the integrals become $N \times N$ tridiagonal matrices that are independent of x and the nodal variables. As a result, the matrices only need to be evaluated once and then can be efficiently stored in computer memory in vector form.

Application of Finite Difference

The streamwise derivatives of $b1_j$ and $b4_j$ are approximated by the finite difference forms

$$\frac{db1_j}{dx} = \frac{b1_j^{n+1} - b1_j^n}{\Delta x} = \frac{\Delta b1_j^{n+1}}{\Delta x}$$

$$\frac{db4_j}{dx} = \frac{b4_j^{n+1} - b4_j^n}{\Delta x} = \frac{\Delta b4_j^{n+1}}{\Delta x} \qquad (21)$$

The superscript n denotes a particular streamwise position where the nodal variables are known. Substitution of the finite difference representations and the introduction of a weighted average for the ordinary differential equations (19) and (20) results in the following formulations:

$$\sum_j^N G1_{kj}\Delta b1_j^{n+1} = \Delta x[\theta D1_k^{n+1} + (1-\theta)D1_k^n] \qquad (22)$$

$$\sum_j^N G2_{kj}\Delta b4_j^{n+1} = \Delta x[\theta D2_k^{n+1} + (1-\theta)D2_k^n]$$

$$\text{for} \quad k = 1, \ldots, N \qquad (23)$$

Here the parameter θ ($0 \le \theta \le 1$) is introduced to control the degree of implicitness. By setting $\theta = 0.5$, as was done in this study, the implicit second-order-accurate Crank-Nicholson scheme is applied.[1] The nodal values are updated using the finite difference formulation (e.g., $b1_j^{n+1} = b1_j^n + \Delta b1_j^{n+1}$).

The quantities $D1_k^{n+1}$ and $D2_k^{n+1}$ are linearized by an expansion about the known position x^n in a manner similar to Ref. 17. Using $D1_k^{n+1}$ as an example, we may write

$$D1_k^{n+1} = \widetilde{D1}_k^n + \frac{d\widetilde{D1}_k^n}{dx}\Delta x + \ldots \approx \widetilde{D1}_k^n + \sum_j^N \frac{d\widetilde{D1}_k^{n+1}}{db1_j^n}\Delta b1_j^{n+1} \quad (24)$$

where the tilde indicates that the nodal values are evaluated at position n, whereas the coefficients l_2 through l_4 are evaluated at position $n+1$. Substituting the linearization of $D1_k^{n+1}$ and $D2_k^{n+1}$ into Eqs. (22) and (23), respectively, results in an implicit noniterative marching scheme:

$$\sum_j^N \left(G1_{kj} - \theta\Delta x \frac{d\widetilde{D1}_k^n}{db1_j^n}\right)\Delta b1_j^{n+1} = \Delta x[\theta D1_k^n + (1-\theta)D1_k^n] \quad (25)$$

$$\sum_j^N \left(G2_{kj} - \theta\Delta x \frac{d\widetilde{D2}_k^n}{db4_j^n}\right)\Delta b4_j^{n+1} = \Delta x[\theta\widetilde{D2}_k^n + (1-\theta)D2_k^n] \quad \text{for} \quad k = 1, \ldots, N \quad (26)$$

Because linear elements were chosen, the stiffness matrices of Eqs. (25) and (26) are tridiagonal and can be efficiently solved by the Thomas algorithm. The nodal variables are evaluated at each streamwise location, without iteration, using a variable step size. Numerical experiments indicate that, in addition to providing adequate accuracy, the marching scheme requires less CPU time than iterating Eqs. (22) and (23) at each streamwise position.

Step Sizing

The variable step size Δx is based on a comparison of the linearized $D1_k^{n+1}$ and $D2_k^{n+1}$ with those calculated after the streamwise step (denoted by an overbar). The relative error is expressed as

$$\lambda = \max\left|\frac{\overline{D1_k^{n+1}} - D1_k^{n+1}}{\overline{D1_k}^{n+1}}\right| \quad \text{or} \quad \max\left|\frac{\overline{D2_k^{n+1}} - D2_k^{n+1}}{\overline{D2_k}^{n+1}}\right| \quad \text{for} \quad k = 1, \ldots, N \quad (27)$$

If the step size has not exceeded assigned limits ($\Delta x_{\min} < \Delta x < \Delta x_{\max}$), then for a minimum and maximum error tolerance ($\lambda_{\min}$ and $\lambda_{\max}$) the step size is halved if $\lambda > \lambda_{\max}$, doubled if $\lambda < \lambda_{\min}$, and unchanged in $\lambda_{\min} \le \lambda \le \lambda_{\max}$. The advantage in using λ is that the user can select the maximum allowable relative error between streamwise steps, and as a result the code avoids nonlinear instabilities in marching. The one drawback with this approach is that the step size can become quite small (1×10^{-4}) in regions of large gradients with respect to x such as those near the leading-edge stagnation point and near the separation point. For this study $\Delta x_{\min} = 1 \times 10^{-7}$, $\Delta x_{\max} = 0.1$, $\lambda_{\min} = 1 \times 10^{-3}$, and $\lambda_{\max} = 1 \times 10^{-2}$.

Results

Laminar and Incompressible

Figure 2 compares the skin friction distribution for the boundary layer about a circular cylinder using 3 and 17 nodes to the classical solution given on page 171 of Ref. 18. As seen, the three-node solution deviates from the classical solution of Blasius-Hiemenz-Howarth in the adverse pressure region. However, the very crude grid presents accurate results in the favorable gradient region.

Figure 3 compares the skin friction distribution for an NACA 0012 airfoil using a full Navier-Stokes solver[19] and the boundary-layer code for 3 and 17 nodes. Conditions are at a Mach number of 0.5, a Reynolds number of 5×10^3, and zero angle of attack. As was shown for the cylinder, the three-node run gives an accurate solution in the favorable pressure gradient region but deviates in the unfavorable region. Notice that the three-node solution does not indicate separation. The 17-node run gives an accurate solution throughout the gradient range. However, it does indicate premature flow separation ($x_s \approx 0.55$). The early separation problem is a result of the lack of interaction between the inviscid and boundary-layer codes. The NACA 0012 test case is considered an encouraging preliminary result.

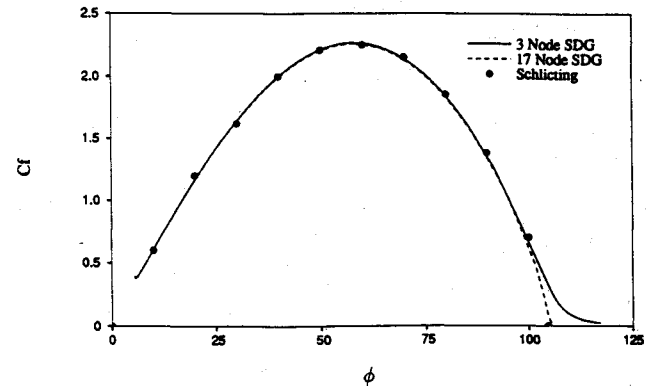

Fig. 2 Computed surface friction coefficient for laminar flow past a cylinder.

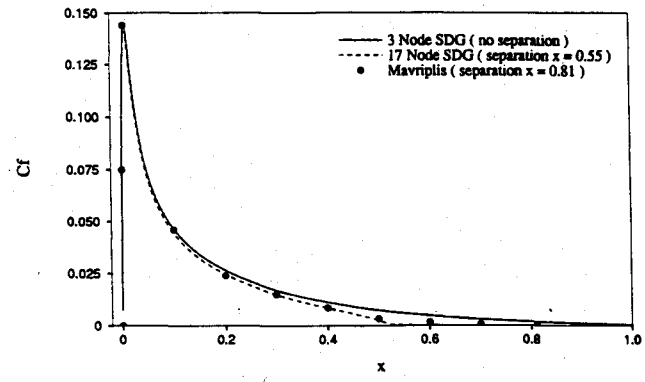

Fig. 3 Computed surface friction coefficient for laminar flow past an NACA 0012 airfoil; $M = 0.5$, $Re = 5 \times 10^3$, and $\alpha = 0$ deg.

Laminar and Compressible

Figure 4 compares the calculated C_f distribution on an adiabatic flat plate through low- to high-compressibility conditions ($0 \le M_\infty \le 10$) with the results shown on page 337 of Ref. 18. The variable ω is used in the power law relating temperature and boundary-layer viscosity:

$$\frac{\mu}{\mu_\infty} = \left(\frac{T}{T_\infty}\right)^\omega \quad (28)$$

The SDG method gives satisfactory results over the entire Mach number range using 17 nodes.

Turbulent and Incompressible

Figure 5 compares the calculated C_f distribution for an adverse pressure gradient with the calculated and experimental results of Refs. 20–22. The 17-node SDG method, with the eddy-viscosity model, gives acceptable results.

Work in Progress

The integral equations (15) and (16) can be reformulated to solve for $\partial\tau/\partial x$ and $\partial s/\partial x$ directly and thereby eliminate the asymptotic behavior of τ and s near the separation point.

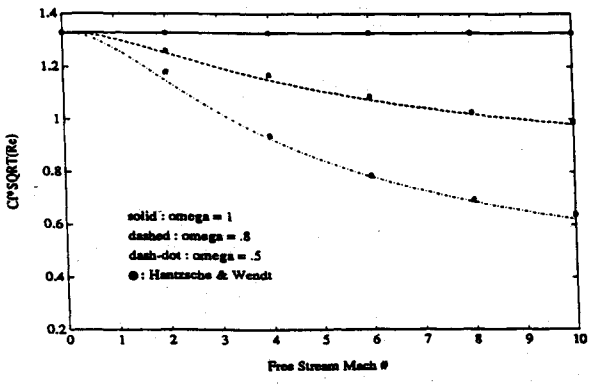

Fig. 4 Surface friction coefficient on an adiabatic flat plate.

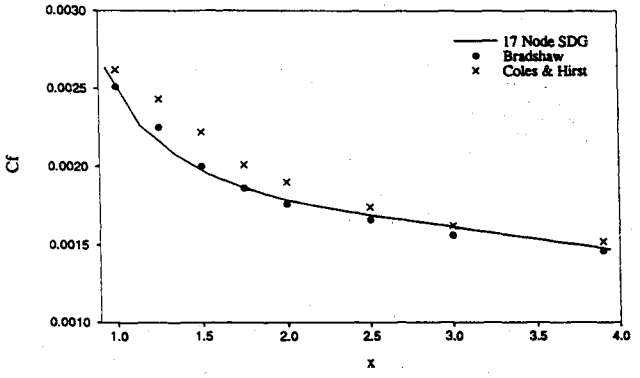

Fig. 5 Surface friction coefficient comparison for an adverse pressure gradient.

Assuming that there is neither surface injection nor suction, the integral of the sum of $\tau^2 f \times$ Eq. (10), $\tau^2 \times df/du_2 \times$ Eq. (11), and $2\tau f \times \partial/\partial\eta \times$ Eq. (11) results in

$$\frac{d}{dx}\int_0^1 f u_2 \tau \, du_2 = l_3 \int_0^1 \tau \frac{\partial}{\partial u_2}[f(1-u_2^2)] \, du_2 + 2Cl_4 \int_0^1 \tau \frac{\partial}{\partial u_2}\left[f\tau \frac{\partial}{\partial u_2}(F\tau)\right] du_2 - Cl_4 \int_0^1 \frac{df}{du_2} \tau^2 \frac{\partial}{\partial u_2}(F\tau) \, du_2 - 2l_3 \int_0^1 f u_2 \tau \, du_2 \tag{29}$$

Equation (16) may be reformulated by taking the integral of the sum of $s\tau f \times$ Eq. (10), $s\tau(df/du_2) \times$ Eq. (11), $\tau f \times$ Eq. (12), and $sf \times \partial/\partial\eta \times$ Eq. (11), which is equal to

$$\frac{d}{dx}\int_0^1 f u_2 s \, du_2 = -4l_3 \int_0^1 f u_2 s \, du_2 + l_3 \int_0^1 \frac{df}{du_2}(1-u_2^2)s \, du_2 + Cl_4 \int_0^1 s \frac{\partial}{\partial u_2}\left[f\tau \frac{\partial}{\partial u_2}(F\tau)\right] du_2 + \frac{Cl_4}{Pr}\int_0^1 f\tau \frac{\partial}{\partial u_2}\left(F\tau \frac{\partial s}{\partial u_2}\right) du_2 + l_2 l_4 \int_0^1 f\tau \frac{\partial}{\partial u_2}(u_2 F\tau) \, du_2 \tag{30}$$

Work continues on the boundary-layer program to incorporate an inviscid code/boundary-layer code interaction model. Two methods of inviscid/boundary-layer interaction are currently under study. For the inviscid flow, both methods will use an innovative Euler equation solver developed by Peter Hartwich at the NASA Langley Research Center. In the first interaction method the displacement thickness is used to generate an "effective body." This involves grid regeneration in the inviscid code. A compressible displacement thickness of the dimensionless form

$$\delta^* = \int_0^\infty \left(1 - \frac{\rho u}{\rho_e u_e}\right) dy \tag{31}$$

has been reformulated to yield

$$\delta^* = \frac{(\gamma+1)}{2\gamma}\frac{u_e}{p_e}\frac{U_\infty}{\sqrt{Re}}\left[\frac{1}{u_e^2}\int_0^1 \frac{(1-u_2)}{\tau} du_2 + \frac{(\gamma-1)}{(\gamma+1)}\int_0^1 u_2 \frac{(1-u_2)}{\tau} du_2 - \int_0^1 \frac{s}{\tau} du_2\right] \tag{32}$$

where the external conditions are given by the inviscid code. The preliminary results using the displacement thickness are encouraging. Application to flow interaction about an airfoil is in progress.

The second interaction method involves the transpiration velocity boundary condition attributed to Lighthill[23] of the compressible form,

$$\bar{v}_t = \frac{a^*}{\rho_e}\frac{\partial(\rho_e u_e \delta^*)}{\partial x} \tag{33}$$

In this development it takes the form

$$v_t = u_e\left[\frac{\partial \delta^*}{\partial x} + \left(l_3 + \frac{1}{\rho_e}\frac{d\rho_e}{dx}\right)\delta^*\right] \tag{34}$$

This may be used as a normal velocity boundary condition imposed at the airfoil surface in the inviscid code. A detailed study is currently being conducted. In addition, extension of the calculations beyond flow separation is being investigated in a manner similar to that outlined by Holt.[24]

Conclusions

Preliminary results have been presented of an accurate and computationally efficient finite element/finite difference method (semidiscrete Galerkin or SDG method) to be used to calculate compressible turbulent boundary-layer flow about airfoils. In this method the group finite element scheme is applied to the Dorodnitsyn formulation of the boundary layer equations. The Dorodnitsyn formulation provides high spatial resolution near the body surface. The finite element discretization across the layer yields a system of first-order ordinary differential equations that automatically follow the boundary-layer growth in the streamwise direction. Linear elements are chosen for computational efficiency, while also providing adequate accuracy. The streamwise derivatives are solved by an implicit and noniterative finite difference marching scheme that allows the user to set the error between steps and avoids nonlinear instabilities. The SDG method and resulting code can be applied to any smoothly connected airfoil shape without modification and can be coupled to any existing inviscid flow solver (portability). A fast, accurate, and computationally efficient inviscid flow solver, coupled with the SDG code, will make an excellent tool for airfoil design.

Acknowledgments

This work was supported under NASA Grant NAG-1-1196. The author would like to thank Stuart Strong of Rice University for his help and Peter Hartwich, Richard Campbell, and Dennis Allison of the NASA Langley Research Center for their many helpful suggestions.

References

[1]Anderson, D. A., Tannehill, J. C., and Pletcher, R. H., *Computational Fluid Mechanics and Heat Transfer,* McGraw-Hill, New York, 1984.

[2]Blottner, F. G., *Computational Techniques for Boundary Layers,* AGARD Lecture Series No. 73, 1975.

[3]Hytopoulos, E., Schetz, J. A., and Gunzburger, M., "Numerical Solution of the Compressible Boundary Layer Equations Using the Finite Element Method," AIAA Paper 92-0666, 1992.

[4]Popinski, Z., and Baker, A. J., "An Implicit Finite-Element Algorithm for the Boundary Layer Equations," *Journal of Computational Physics,* Vol. 21, 1976, pp. 55–84.

[5]Baker, A. J, and Manuhardt, P. D., "Numerical Prediction of Mean and Fluctuating Velocities for Jet-Flap Flows," *AIAA Journal,* Vol. 16, No. 8, 1978, pp. 807–814.

[6]Fletcher, C. A. J., and Fleet, R. W., "A Dorodnitsyn Finite Element Formulation for Laminar Boundary Layer Flow," *International Journal of Numerical Methods in Fluids,* Vol. 4, 1984, pp. 399–419.

[7]Fletcher, C. A. J., and Fleet, R. W., "A Dorodnitsyn Formulation for Turbulent Boundary Layers," *Computers and Fluids,* Vol. 12, 1983, pp. 31–45.

[8]Meade, A. J., "Semidiscrete Galerkin Modeling of Compressible Viscous Flow Past an Airfoil," NASA CR 182092, pp. 86–87.

[9]Fletcher, C. A. J., "The Group Finite Element Formulation," *Computational Methods in Applied Mechanics and Engineering,* Vol. 37, 1982, pp. 225–243.

[10]Dorodnitsyn, A. A., "General Method of Integral Relations and Its Application to Boundary Layer Theory," *Advanced Aerospace Sciences,* Vol. 3, 1962, pp. 207–219.

[11]Cebeci, T., and Smith, A. M. O., *Analysis of Turbulent Boundary Layers,* Academic Press, New York, 1974.

[12]Van Driest, E. R., *Journal of Aeronautical Sciences,* Vol. 23, 1956, pp. 1007–1011, 1036.

[13]Clauser, F. H., *Journal of Aeronautical Sciences,* Vol. 21, 1954, pp. 91–180.

[14]Clauser, F. H., *Advanced Applied Mechanics,* Vol. 4, 1956, pp. 1–51.

[15]Chapman, D. R., and Rubesin, M. W., "Temperature and Velocity Profiles in the Compressible Laminar Boundary Layer with Arbitrary Distribution of Surface Temperature," *Journal of Aeronautical Sciences,* Vol. 16, 1949, pp. 547–565.

[16]Brebbia, C. A., and Dominguez, J., *Boundary Elements: An Introductory Course,* McGraw-Hill, New York, 1979.

[17]Briley, W. R., and McDonald, H., "Solution of the Multi-Dimensional Compressible Navier-Stokes Equations by a Generated Implicit Method," *Journal of Computational Physics,* Vol. 24, 1977, pp. 372–397.

[18]Schlichting, H., *Boundary Layer Theory,* McGraw-Hill, New York, 1979.

[19]Radespiel, R., "A Cell-Vertex Multigrid Method for the Navier-Stokes Equations," NASA TM 101557, 1989.

[20]Fletcher, C. A. J., *Computational Techniques for Fluid Dynamics,* Vol. II, Springer-Verlag, New York, 1988, p. 221.

[21]Bradshaw, P., National Physical Lab., Aero Rept. 1219, 1967.

[22]Coles, P., and Hearst, E., *Computation of Turbulent Boundary Layers,* Vol. 2, Stanford Univ., Stanford, CA, 1968.

[23]Lighthill, M. J., "On Displacement Thickness," *Journal of Fluid Mechanics,* Vol. 4, 1958, pp. 383–392.

[24]Holt, M., *Numerical Methods in Fluid Dynamics,* Springer-Verlag, New York, 1984, pp. 149–153.